Journal of Materials Science: Materials in Electronics (2019) 30:19164–19172
https://doi.org/10.1007/s10854-019-02273-1

Structural characteristics and electrochemical properties of sulfonated polyimide clay-based composite fabricated by a solution casting method

Nisar Ali[1,2] · Farman Ali[3] · Shaukat Saeed[4] · Syed Sakhawat Shah[3] · Muhammad Bilal[5]

Received: 10 July 2019 / Accepted: 24 September 2019 / Published online: 1 October 2019

Abstract

Herein, the electrochemical and structural properties of sulfonated polyimide (SPI) clay-based composite films have been investigated. SPI reinforced with grafted sonicated clay (GSC) was fabricated via a solution casting method in the form of thin films. The as-synthesized thin films were light brown, tough, flexible and transparent. The thickness of the films were 0.109 mm and 0.056 for pristine SPI and GSC-SPI, respectively. The fabricated composite was fully investigated via Fourier transform infrared spectroscopy (FTIR), proton nuclear magnetic resonance spectroscopy (^{1}H NMR), carbon (^{13}C) NMR and impedance spectroscopy. The completion of the proton exchange reaction was confirmed by ^{1}H NMR. The electrical properties of the SPI-clay based composite film were investigated by impedance spectroscopy. The conductivity was measured in a wide frequency range from room temperature to 363 K by applying an *ac* signal of 0.5 V. The appearance of two semicircular arcs at low and high frequency shows two conduction mechanisms with different relaxation times at the exterior and interior of the system. Bode plot also confirms the presence of two electro-active regions. The shift in the position of tanδ peaks to lower frequency region with increasing temperature shows that these relaxations are thermally deactivated. The *ac* conductivity of the system increased from 6.02E−10 for neat SPI to 6.61E−6 Ω^{-1} cm^{-1} for SPI-GSC composite. In conclusion, these layered silicates based conductive films have the potential to act as a polyelectrolyte membrane for fuel cell energy devices.

1 Introduction

Sulfonated polyimide reinforced with layered silicates provides a well-known category of organic–inorganic nanocomposites with admirable mechanical, thermal and transport properties [1–4]. Reinforcement of the inorganic fillers to the membrane made from polymer has enticed many researchers because of the low cost, better thermal stability and high hydrophilicity [5, 6]. To increase the stability, proton conductivity with barrier properties, the combination of polymer membrane with silicates can lead to the reduction in cost and improve the water retention property of prepared composite membranes [6–8]. In spite of that, the organic/inorganic phase interaction and the degree of dispersion may play an indispensable role in the enhancement of the membrane properties [9].

Recently, considerable efforts and research work are in progress to achieve well functionalization of clays by grafting reactions [10, 11]. Organo-clays prepared by the grafting method show excellent structural, thermal and chemical stability because of the clay matrix and grafted molecules have strong covalent linkages. Organosilanes have the property to be adsorbed on the external surfaces of clay mineral by hydrogen bonding. Due to the larger size of organosilane molecules, this needs rigorous reaction conditions to achieve the grafting of the interlayer. These include the solvent of pure organosilane, high reaction temperatures, and inert environment [12–14].

✉ Nisar Ali
nisar.ali@tdtu.edu.vn

✉ Farman Ali
farmanqau@gmail.com

1 Department for Management of Science and Technology Development, Ton Duc Thang University, Ho Chi Minh City, Vietnam

2 Faculty of Applied Sciences, Ton Duc Thang University, Ho Chi Minh City, Vietnam

3 Department of Chemistry, Hazara University, Mansehra 21300, Pakistan

4 Department of Metallurgy and Materials Engineering (DMME), PIEAS, PO Nilore, Islamabad 45650, Pakistan

5 School of Life Science and Food Engineering, Huaiyin Institute of Technology, Huai'an 223003, China

Among different matrix materials, sulfonated polyimides have gained much attention as they are frequently used in various technological applications [15–17]. Recently, extensive research work has been done on the membrane of sulfonated polyimide, which is clear from the high level of publications and patents, particularly in the application in fuel cell [15, 18]. Chang et al. [19] carried out in situ polymerizations of SPTA under click chemistry via propargyl-functional modified clay for the preparation and characterization of sulfonated polytriazole-clay (SPTA-clay) nanocomposites. Chirachanchai et al. [7] used poly (ether ether ketone) (SMMT/SPEEK) montmorillonite/sulfonated for the preparation organic–inorganic nanocomposite membrane. SMMT was modified with silane consisting proton conductivity of a sulfonic acid group. Atif et al. used poly(vinyl alcohol) and aqueous solutions of chitosan and crosslinker (tetraethoxysilane (TEOS)) for the preparation of polymer films and also employed to investigate its effect on the electrical properties of polymer blends [20]. Yuan et al. investigated the electrical properties of a new cross-linked naphthalenic polyimide using impedance spectroscopy [8].

In the present work, sulfonated polyimide/clay-based composites have been fabricated and their electrical and structural properties have been investigated. The dispersion and interaction between sulfonated polyimide matrix and clay particles have been enhanced by surface modification of clay particles. The main emphasis was to study the electrical properties of the composite using impedance spectroscopy. As the impedance spectroscopy evaluate the material dielectric properties [12, 21], in which imaginary and real parts of complex material are characterized as a function of the applied electric field frequency [22]. It defines the outer field interaction with the electric dipole moment of the material. This method is now being extensively used in many of scientific field's, for example, polyelectrolyte membrane (PEM) testing and characterization of microstructures. Herein, we present the fabrication of organo-functionalized clay-based conducting composite in the form of thin films having intercalated networks of (layered silicates). The SPI/GSC thin films were characterized using FT/IR (Fourier transform infrared spectroscopy), ^{13}C NMR and ^{1}H NMR spectroscopy. To study the electrical properties of SPI/GSCthin film we used the technique of impedance spectroscopy. These conductive films of layered silicates may have potential application as PEM for fuel cell energy devices.

2 Experimental

2.1 Synthesis of the sulfonated polyimide

Sulfonated polyimide (SPI) was prepared via a chemical imidization method. A stoichiometric amount of 4,4-diamino diphenyl ether-2,2-disulfonic acid (ODADS) was dissolved in *m*-cresol under an inert environment. Upon complete dissolution of ODADS, 1,4,5,8-naphthalene tetracarboxylic dianhydride (NTDA) was added and the resultant mixture was treated at 80 °C for 4 h followed by additional heating at 180 °C and 20 h time interval to complete the imidization reaction. Synthetic details of SPI and their corresponding nanocomposites has been given in our previous report [23].

2.2 Synthesis of grafted sonicated vermiculite clay

The grafting of vermiculite (VMT) with 3-aminopropyl triethoxysilane (3-APTES) was carried out using the ultrasonic processor of sonic and material (Model-VC 505-350) with 20-kHz converter coupled to a titanium probe. Adequately, 2 wt % of 0.9 g of sodium vermiculite clay [24] was suspended in 50 mL of toluene. Argon gas was bubbled under stirring for 6.0 h. The linker, 3-aminopropyl triethoxysilane (3-APTES) (6.2 mL) was dropwise introduced to the reaction mixture and sonicated from 10 to 30 min. Grafted vermiculite clay from the suspension was recovered by filtration and then, repeatedly washed with ethanol to remove any residual APTES. The sample was dried in a vacuum oven at 120 °C for 12 h to acquire grafted sonicated vermiculite clay.

2.3 Synthesis of SPI-clay based composite

The synthesized SPI was re-dissolved in dimethyl sulfoxide (DMSO) via heating at 80 °C, accompanied by vigorous stirring. A weighted amount of 5 wt % GSC was added to the polymer solution and the reaction mixture was sonicated in an ultrasonic bath [frequency (35 kHz)] for 5 h with the temperature maintained at 25 °C by the help of a cooling circuit to ensure uniform dispersion of clay. A schematic illustration of the reaction between the SPI and the clay (GSC) is depicted in Fig. 1.

2.4 Characterization

The following section contains details about the techniques used for the structural and electrical analysis of the developed materials.

2.4.1 Proton (^{1}H) NMR

Structure elucidation of SPI (in salt form) was carried out using ^{1}H NMR. The spectra were recorded on CPMAS-Bruker Advance II spectrometer at 300 and 75 MHz using DMSO as a solvent.

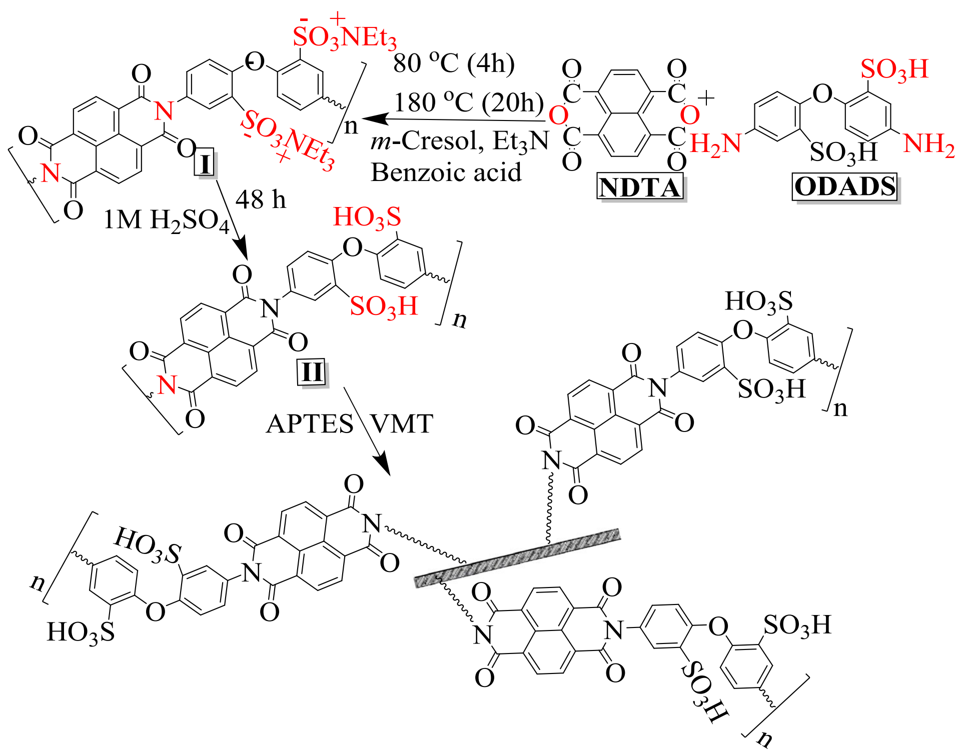

Fig. 1 Schematic illustration for the reaction between the SPI and GSC

2.4.2 Carbon (^{13}C) NMR

Structural interpretation of the sulfonated diamine (ODADS) was carried out using ^{13}C solid-state NMR. The spectra were recorded on CPMASBruker Advance II spectrometer at 300 and 75 MHz.

2.4.3 Electrical properties

Impedance spectroscopy was used to measure the electrical properties, whereas Alpha-N analyzer (Novo control, Germany) in the frequency range of 1×10^{-1} Hz to 1×10^{7} Hz was used for the conductivity measurements. Films were (10 mm × 10 mm) were cut in the proper size and linked using wires on the films by silver paste and cured at 120 °C temperature for 2 h of time to vanish the presence of any humid drop. The data was accomplished using WINDETA software having fully automated interface of analyzer [25].

2.4.4 Fourier transform infra-red spectroscopy

Diffuse Reflectance Infrared Fourier Transform (DRIFT) spectroscopic analysis was performed using Thermo Scientific Nicolet IS10 spectrometer, while the scanning coverage was from 4000 to 400 cm^{-1} with a 4 cm^{-1} spectral resolution and averaged over 60 scans.

3 Results and discussion

3.1 ^{1}H NMR

Figure 2 illustrates the ^{1}H NMR spectrum of SPI in triethylammonium (salt) form. No residual protons of amide or carboxylic acid were observed, signifying the successful completion of imidization reaction [26]. The protons of methyl group appear as a singlet about 1 ppm, while proton of the methylene group resonates as a doublet at 2.54 ppm. The peak for –NH proton appears as a singlet of two protons at 3.35 ppm, whereas the peak at 7.171 ppm is for proton at C-1 of the phenyl ring, appears as a triplet because of its coupling with a proton at C-2 and C-3. The peak at 7.9 ppm is for proton at C-2 of phenyl ring that appears as a doublet due to its coupling with a proton at C-1. The peak at 8.4 ppm appears as a broad singlet, which is attributed to the proton at C-3 of the phenyl ring. The peak at 9.2 ppm appears as a singlet for the proton of naphthalenic dianhydride. The above data confirm the successful synthesis of SPI polymer via one-step chemical imidization method.

3.2 FTIR of SPI and SPI-clay hybrid membranes

Figure 3 displays the FTIR spectra of SPI and composite having 5% GSC clay. The appearance of an absorption band of the amide group around 1717 cm^{-1} (asymmetric) and 1672 cm^{-1} (symmetric) indicates the successful preparation

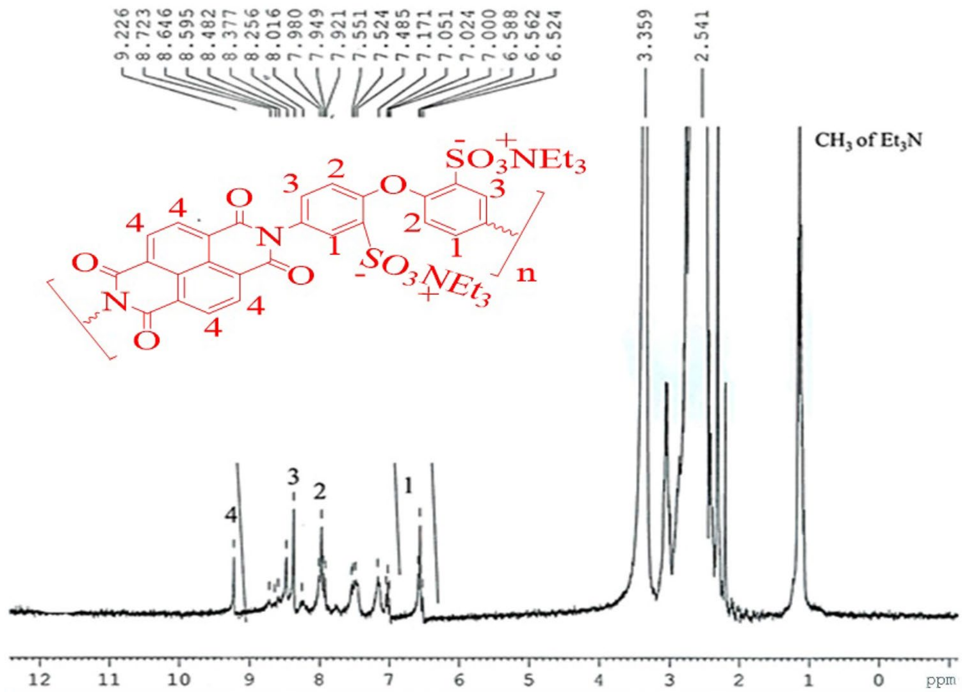

Fig. 2 [1]H NMR spectra of SPI in (salt form)

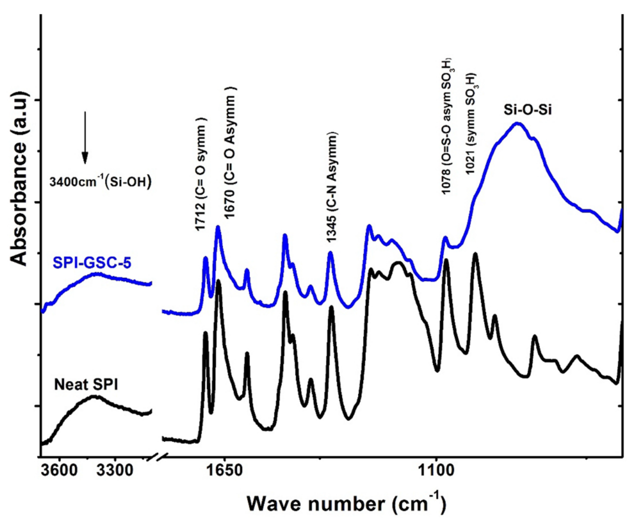

Fig. 3 FTIR spectra of neat SPI and SPI-GSC composite

of the SPI-clay hybrid membranes [12, 27]. The C-N stretching vibration of the amide ring was observed at 1345 cm^{-1}. The presence of these bands indicates the formation of amide [27]. Lacking any absorbance peaks around 1650 cm^{-1} and 1550 cm^{-1} substantiates the complete imidization [28]. Sulfur-oxygen symmetric vibration (O=S=O) and asymmetric stretching of the sulfonic acid groups appeared at 1078 cm^{-1} and 1021 cm^{-1} [29–31]. The appearance of a broader band at 830–1030 cm^{-1} was assigned to the O–Si–O stretching vibration of GSC clay. An extensive absorption band at 3400 cm^{-1} was attributed to Si–OH of the silicates. Overall, the FTIR analysis confirmed the successful synthesis of SPI and GSC-based composites [32].

4 ^{13}C NMR of sulfonated diamine

Figure 4 presents the structural elucidation of the prepared sulfonated diamine. The carbon-6 (C6) of the phenyl adjacent to the amine group appears at 152.9 ppm, this higher de-shielding value is most probably due to the amino group (EWG) present at C6. The other peak, which appears at 133.6 ppm, is for C5 present at the ether linkage. The peak at 127 ppm is assigned to C4 linked to the sulfonic acid group. The signal of C3 and C2 appear at 125 and 120 ppm, respectively, while C1 resonates at 118 ppm i.e. the region representing aromatic carbons. All these findings corroborate the successful sulfonation of ODA to ODADS.

4.1 Charge transport properties

Impedance spectroscopy analysis of the fabricated thin films was studied in the 1×10^{-1} Hz to 1×10^{7} Hz frequency range at elevated temperatures. Equation 1 explain the complex impedance (z*) [33].

$$z^* = z' + jz'' \tag{1}$$

where z′ is the real part of impedance, the z″ is imaginary part of impedance, and j is the imaginary number equal to $\sqrt{-1}$. The Nyquist plots (temperature range 35 to 55 °C) of SPI-clay based composite film at low and high frequency

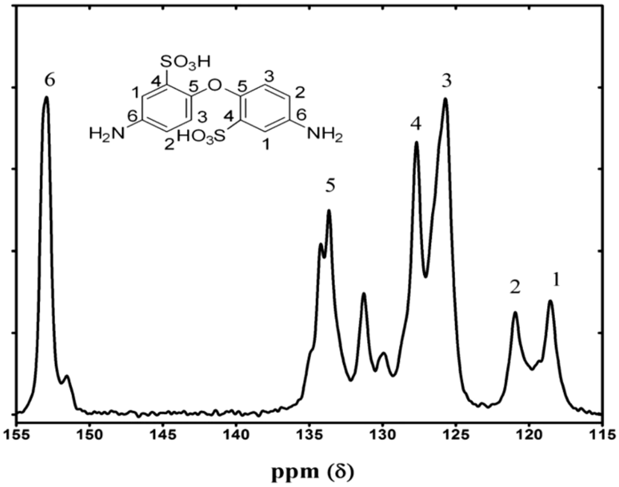

Fig. 4 ^{13}C CPMAS NMR spectrum of the synthesized SPI

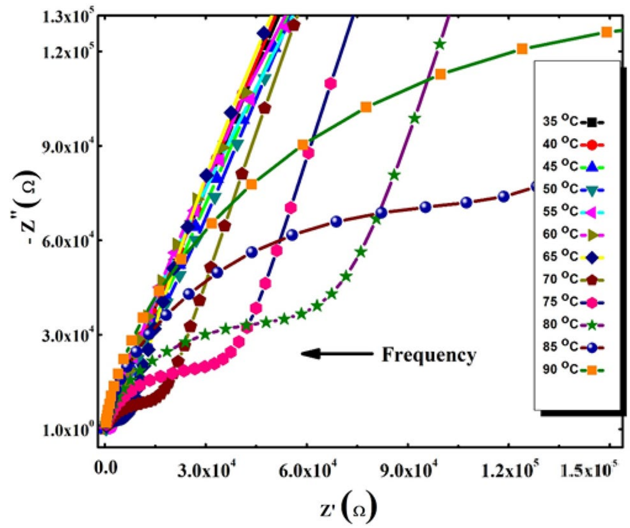

Fig. 6 Nyquist plot of SPI-clay based composite at different temperatures

are demonstrated in Figs. 5 and 6, respectively. The plot shows apparently a single semi-circular *arc* (Fig. 5) in a temperature range of 55 °C. Beyond this temperature range, two semicircular *arcs* were observed, and radii of semicircular *arcs* increased with increase in temperature. The *arc* at low frequency is due to the relaxation of charge carriers at some trapping sites such as grain boundaries and other defects in the system [34]. The radii of these semicircular *arcs* (both at low and high frequency) are directly related to the resistance of the system [35]. A further increase in temperature up to 90 °C causes both semicircular *arcs* to shift toward lower frequencies indicating that the charge carriers are delocalized [34]. It can be concluded that the semicircular *arcs* at low and high frequency show two conduction mechanisms with different relaxation times at the exterior and interior of the system, respectively. Below 55 °C, the core charge carriers do not contribute to conduction of the system. However, as the temperature increases, these charges gain some thermal energy (kT) and become available for conduction. Due to this reason, the radii of both semicircular *arcs* increases, indicating that the conductivity of the system decreases with increase in temperature [34].

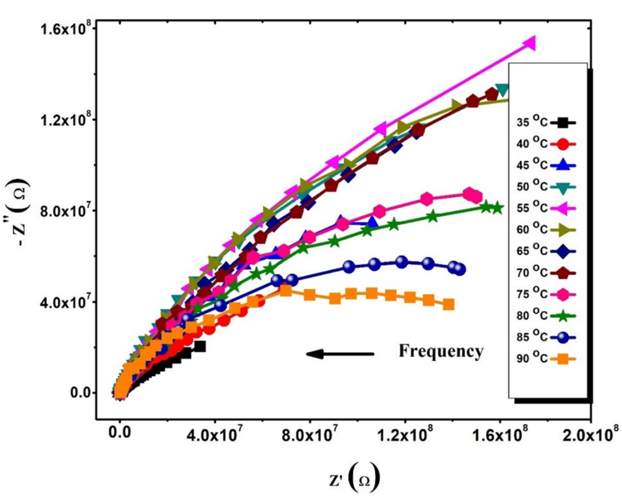

Fig. 5 Nyquist plot of SPI-clay based composite at different temperatures

The Borde plot for the imaginary part of the complex impedance as a function of frequency shows two peaks at 10 Hz and 10^6 Hz (Fig. 7). The height of the peak specifies total resistance of the electro-active region in the system, while the position of the peak (relaxation frequency) shows the ability of charge carriers in the system. The Bode plot is in agreement with the Nyquist plot, which shows two electro-active regions. The one at low frequency is due to the grain boundaries in the system, while the second is due to the core region surrounded by grain boundaries and various defects. Hence, there are two relaxation phenomena with different relaxation times ($\tau = RC$). The relaxation time of the charge carriers at grain boundaries is larger as compared to that of the core relaxation time. This is due to the large resistance of the grain boundaries and other interfaces [34]. It can be observed that the height of both peaks increases with increasing temperature. This reveals that both phases become more resistive with increasing temperature [35]. Moreover, both peaks shift toward low frequency, which indicates that there is only metallic conduction and no possibility of the band or hopping conduction. This may be due to the presence of various free metal ions in the clay [24]. The conduction mechanism indicates that the metal ions are completely free and bonded neither ionically nor covalently. The use of conventional complex impedance plane plots in an inhomogeneous material gives very limited information, as these plots are dominated by the most resistive regions

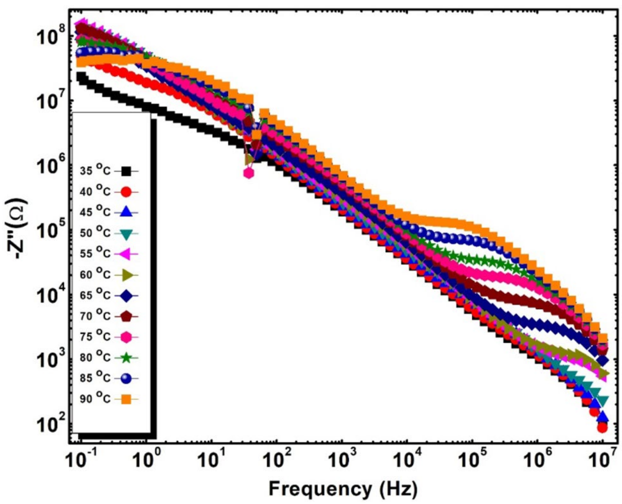

Fig. 7 Spectroscopic plot of SPI-clay based composite at different temperatures

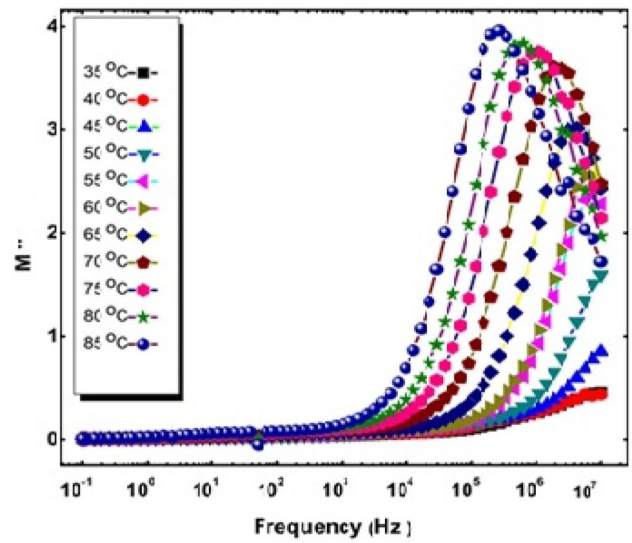

Fig. 8 (M″) vs. frequency plot of SPI-clay based composite

and are insensitive to the more conductive regions within a sample. The complex impedance is defined in Eq. 2 [36]

$$M^{*}(\omega) = 1/\varepsilon(\omega) = M' + jM'' = j\omega C_0 Z^{*} \quad (2)$$

where the real part of modulus $M' = j\omega C_0 Z''$ and imaginary part of modulus is $M'' = j\omega C_0 Z'$, $\omega = 2\pi f$ is the angular frequency, ε^{*} is permittivity, and Z^{*} is complex impedance. $C_0 = \varepsilon_0 A/t$ is capacitance, ε_0 is permittivity of free space, A is an area of the electrode surface, and t is thickness. To probe this phenomenon, combined spectroscopic plots of the imaginary components of modulus M" are plotted as a function of frequency in Fig. 8. The special character of this plot is that it marks the most resistive part of the system and provides detailed information about the most electro-active region. In our case, the most conductive region is the core region, which response at high frequency. This is the reason that we can see the peaks at high frequency while the low-frequency resistive region is masked. A single peak in the spectrum is observed at each temperature.

The frequency at which the maximum of the peak occurs is called relaxation frequency. It is well defined from the plot that the relaxation frequency shifts towards low-frequency values as the temperature increases. This shift in the relaxation frequency reveals that the charge carriers are de-localized and conductivity decreases with increase in temperature [37]. The height of the peak slightly increases with increase in temperature.

Figure 9 shows the variation of tanδ, which is also defined as a dielectric loss, as a function of frequency at different temperatures for SPI-clay based composites sample. Each spectrum possesses only one peak, which corresponds to a single relaxation; it can be observed that all peaks are shifted to a lower frequency region with an increase in temperature.

This shift in the position of tanδ peaks to lower frequency side (Fig. 9) with increasing temperature shows that these relaxations are thermally deactivated. An increase in the magnitude of tanδ is observed which may be due to the scattering and continues collision of the charge carries with each other and with atoms of the clay [38–40].

The temperature-dependent relaxation time at various temperatures is calculated using Eqs. 3 and 4.

$$T = 1/2\pi f_{\max} \quad (3)$$

$$\tau = \tau_o e^{Ea/RT} \quad (4)$$

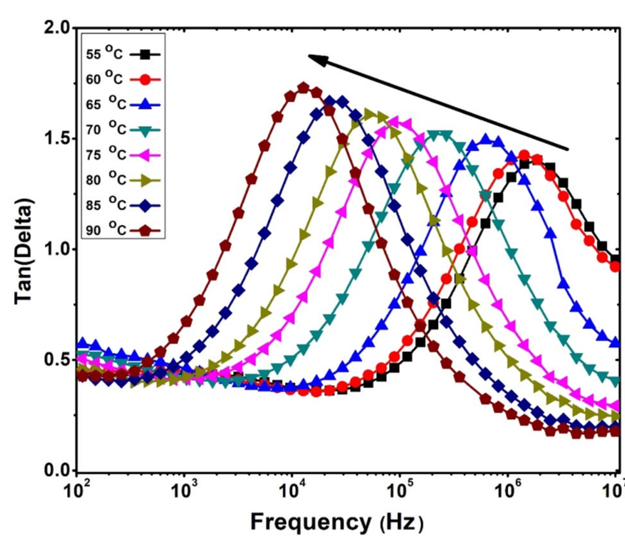

Fig. 9 Tan δ of SPI-clay based composite at different temperatures

where E_a is the activation energy (kJ mol^{-1}), R is the ideal gas constant (J mol^{-1} K^{-1}) and T the temperature (K). The negative activation energy again vanishes, the possibility of semiconducting or insulating nature of the system. Hence, there is no band or hopping conduction mechanisms (Fig. 10).

4.2 Dielectric response

Like complex impedance, dielectric constant also has real (ε') and imaginary part (ε''). The real part of dielectric constant shows the energy stored in the system as polarization while the imaginary part demonstrates the energy loss under the applied electric field. The dielectric constant vs. frequency plot is shown in Fig. 11. The plot shows two dispersion regions at a lower and higher frequency, where the dielectric constant decreases with frequency. In the given plot, the real dielectric constant shows two dispersion regions against the frequency. The high dielectric constant at lower frequency is the interfacial polarization, while the second dispersion at comparatively high frequency is the intrinsic dielectric constant of the material. The overall dielectric constant decreases with increasing temperature as indicated in Fig. 11.

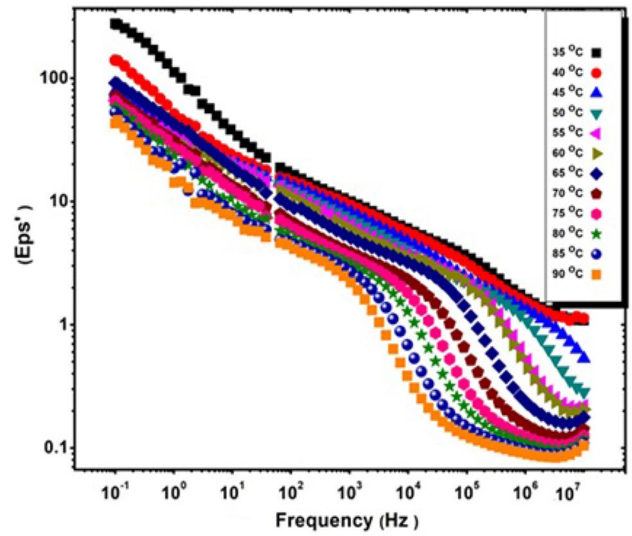

Fig. 11 Dielectric constant (ε′) vs. frequency plot clay based composite

5 Conclusion

The sulfonated polyimide was synthesized via a one-step direct temperature imidization method. The VMT clay was organically modified with 3-APTES using sonication as a tool. The SPI-clay based composite was fabricated by a solution casting method. Electrical characterization reveals that the conductivity SPI-clay decreases with an increase in temperature. However, the overall conduction mechanism of the system is metallic due to the presence of free metallic ions in the system. The Nyquist plot demonstrates that the conduction due to the interface or grain boundaries is dominant throughout the frequency range below 55 °C. While above this temperature, the core charge carries and/or ions become free by gaining thermal energy and contribute in conduction of the system. The core conduction appears as a second semicircular arc above 55 °C at high frequency. The combined spectroscopic plots of the imaginary components of an imaginary part of the modulus M'' and frequency shows a single peak in the spectrum of all temperatures, representing the most conductive core region. It is observed that the relaxation frequency of the Modulus peaks shifts towards low-frequency values as the temperature increases. This shift in the relaxation frequency reveals that the charge carriers are de-localized which provide further evidence for the presence of metallic conduction and delocalization of charge carriers. The dielectric plot shows two dispersion regions against the frequency, the high dielectric constant at lower frequency is the interfacial polarization, while the second dispersion at comparatively high frequency is the intrinsic dielectric constant of the material. The *ac* conductivity was also calculated which increases from 6.02E−10 for neat SPI to 6.61E−6 Ω^{-1} cm^{-1} for SPI-GSC composite. In conclusion, these composite films could be used as a polyelectrolyte membrane in fuel cell devices for the production of clean energy.

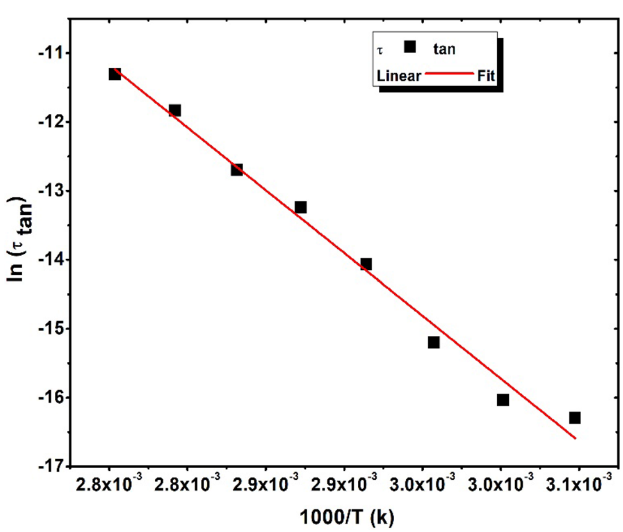

Fig. 10 The relaxation time ln (τ_{Tan}) against inverse temperature (1000/T)

Acknowledgements The authors also acknowledge the support from Postgraduate Research & Practice Innovation Program of

Jiangsu Province (SJCX17_0700), and Young academic leaders in Jiangsu Province, Six-talent peaks project in Jiangsu Province (2015-SWYY-026).

Compliance with ethical standards

Conflicts of interest The authors report no conflicting interest in any capacity, competing or financial.

References

1. J. Iqbal, A. Numan, S. Rafique, R. Jafer, S. Mohamad, K. Ramesh, S. Ramesh, High-performance supercapattery incorporating ternary nanocomposite of multiwalled carbon nanotubes decorated with Co_3O_4 nanograins and silver nanoparticles as electrode material. Electrochim. Acta **278**, 72–82 (2018)
2. F. Ran, Y. Tan, Chapter 7-Polyaniline-based composites and nanocomposites, in *Polyaniline Blends, Composites, and Nanocomposites*, ed. by P.M. Visakh, C.D. Pina, E. Falletta (Elsevier, Amsterdam, 2018), pp. 175–208
3. R. Shrivastava, S. Saxena, S.P. Satsangee, R. Jain, Graphene/TiO_2/polyaniline nanocomposite based sensor for the electrochemical investigation of aripiprazole in pharmaceutical formulation. Ionics **21**(7), 2039–2049 (2015)
4. P.M. Visakh, Chapter 1-Polyaniline-based blends, composites, and nanocomposites: state of the art, new challenges, and opportunities, in *Polyaniline-Based Composites and Nanocomposites*, ed. by P.M. Visakh, C.D. Pina, E. Falletta (Elsevier, Amsterdam, 2018), pp. 1–22
5. K.A. Ibrahim, Synthesis and characterization of polyaniline and poly(aniline-co-o-nitroaniline) using vibrational spectroscopy. Arabian J. Chem. **10**, 2668–2674 (2017)
6. S. Shahabuddin, A. Numan, M.M. Shahid, R. Khanam, R. Saidur, A.K. Pandey, S. Ramesh, Polyaniline-$SrTiO_3$ nanocube based binary nanocomposite as highly stable electrode material for high performance supercapaterry. Ceram. Int. **45**, 11428–11437 (2019)
7. V. Elena, P. Gérald, G. Claude, M. Régis, P. Michel, Sulfonated polyimides as proton conductor exchange membranes: physicochemical properties and separation H+/Mz+by electrodialysis comparison with a perfluorosulfonic membrane. J. Memb. Sci. **160**, 127 (1999)
8. M.K. Ananta, B. Saswata, K. Tapas, K.N. Hoon, L.H. Joong, Silicate-based polymer-nanocomposite membranes for polymer electrolyte membrane fuel cells. Prog. Poly. Sci. **37**, 842 (2012)
9. A.R. Vaia, R. Krishnamoorti, *Polymer Nanocomposites: Synthesis Characterization and Modeling* (Amer. Chem. Soc, Washington, DC, 2001)
10. G. Sandip, S. Arindam, M. Sudhangshu, J. Tushar, role of solvent protic character on the aggregation behavior of polybenzimidazole in solution. J. Phys. Chem. **115**, 11474 (2011)
11. G. Zhang, Z. Zhou, Organic/inorganic composite membranes for application in DMFC. J. Memb. Sci. **261**, 107 (2005)
12. H.J. Yao, Y. Yun, S.J. Yu, H.J. Bing, C.C. Feng, Synthesis and characterization of sulfonated polytriazole-clay proton exchange membrane by in situ polymerization and click reaction for direct methanol fuel cells. J. Power Sour. **208**, 144 (2012)
13. B.D. Miracle, L. Donaldson, *Composites*, vol. 21 (ASM International, Materials Park, 2001)
14. Y.S. Qin, Y. Peng, H.H. Ping, Q.H. Zong, Z. Qing, Z.X. Jian, L. Dong, Modeling drug release from a layered double hydroxide–ibuprofen complex. Appl. Clay Sci. **62**, 8 (2012)
15. H. Hongping, J. Duchet, J. July, G.F. Jean, Grafting of swelling clay materials with 3-aminopropyltriethoxysilane. J. Colloid Interface Sci. **288**, 171 (2005)
16. H. Kobayashi, T. Matsunaga, Amino-silane modified superparamagnetic particles with surface-immobilized enzyme. J. Colloid Interface Sci. **141**, 505 (1991)
17. K. Tonle, T. Diaco, E. Ngameni, C. Detellier, nanohybrid kaolinite-based materials obtained from the interlayer grafting of 3-aminopropyltriethoxysilane and their potential use as electrochemical sensors. Chem. Mater. **19**, 6629 (2007)
18. K. Tonle, S. Letaief, E. Ngameni, A. Walcarius, C. Detellier, Square wave voltammetric determination of lead(II) ions using a carbon paste electrode modified by a thiol-functionalized kaolinite. Electroanalysis **23**, 245–252 (2011)
19. Y. Wang, K. Chen, J. Mishler, S. Cho, X.C. Adroher, A review of polymer electrolyte membrane fuel cells: technology, applications, and needs on fundamental research. Appl. Energy **88**, 981 (2011)
20. R. Eto, A. Tanioka, Characteristic proton transport through composite membrane composed of quaternary-amino poly(sulfone) and sulfonated Co-poly(styrene and divinylbenzene). J. Colloid Interface Sci. **200**, 59 (1998)
21. R. Gosalawit, S. Chirachanchai, S. Shishatskiy, P. Nunes, Sulfonated montmorillonite/sulfonated poly(ether ether ketone) (SMMT/SPEEK) nanocomposite membrane for direct methanol fuel cells (DMFCs). J. Memb. Sci. **323**, 337 (2008)
22. Y. Atif, A. Tariq, J. Muhammad, I. Zahid, S. Aneela, S. Misbah, K. Shahzad, J. Tahir, J. Solid State Electron. **20**, 571 (2015)
23. Y. Sen, R. Carmen, L. Mar, G. Xiaoxia, F. Jianhua, R. Evaristo, Impedance spectroscopy and performance of cross-linked new naphthalenic polyimide acid membranes. J. Phys. Chem. C **114**, 22773 (2010)
24. S. Ray, S. Uprakas, B. Mosto, Biodegradable polymers and their layered silicate nanocomposites: in greening the 21st century materials world. Prog. Mater Sci. **50**, 962 (2005)
25. J. Potter, *U.-S Geological Survey Minerals Year book*. (2003)
26. K. Zhang, J. Xu, Y. Wang, L. Cheng, J. Wang, B. Liu, Preparation and characterization of chitosan nanocomposites with vermiculite of different modification. Polym. Degrad. Stab. **94**, 2121–2127 (2009)
27. A.B. Afzal, M.J. Akhtar, Effect of inorganic silver nanoparticles on structural and electrical properties of polyaniline/PVC blends. J. Inorg. Org. Poly. Mater. **20**, 783 (2010)
28. A. Farman, S. Shaukat, S.S. Syed, R. Fazal, D. Laurent, L.M. Jean, R. Laurence, Sulfonated polyimide-clay thin films for energy application. Recent Pat. Nanotechnol. **10**, 221 (2016)
29. E.M. Ali, A.M. Kumar, B. Susanta, Synthesis and characterization of new fluorinated poly(ether imide) copolymers with controlled degree of sulfonation for proton exchange membranes. J. Membr. Sci. **411**, 117–129 (2012)
30. T. Wang, F. Sun, H. Wang, S. Yang, L. Fan, Preparation and properties of pore-filling membranes based on sulfonated copolyimides and porous polyimide matrix. Polymer **53**, 3154–3162 (2012)
31. C. Kangcheng, H. Zhaoxia, E. Nobutaka, H. Mitsuru, O.I. Ken, Sulfonated multiblock copolynaphthalimides for polymer electrolyte fuel cell application. Polymer **52**, 2255–2262 (2011)

32. J. Wonbong, S. Saimani, C. Seunghyuk, S.G. Yong, H. Haksoo, Acid–base polyimide blends for the application as electrolyte membranes for fuel cells. J. Membr. Sci. **280**, 321–329 (2006)
33. N. Feifei, P. Jennifer, J. Deborah, R. Jacques, Synthesis of novel proton-conducting highly sulfonated polybenzimidazoles for PEMFC and the effect of the type of bisphenyl bridge on polymer and membrane properties. J. Polym. Sci., Part A: Polym. Chem. **49**, 2107–2117 (2011)
34. S. Chen, Y. Yin, H. Kita, I. Okamoto, Synthesis and properties of sulfonated polyimides from homologous sulfonated diamines bearing bis(aminophenoxyphenyl)sulfone. J. Polym. Sci., Part A: Polym. Chem. **45**, 2797–2811 (2007)
35. E. Barsoukov, R. Macdonald, *Impedance Spectroscopy Theory, Experiment and Applications* (Wiley, New York, 2005)
36. A. Flores, F.C.J. Balta, I.G.D. Marco, S. Sturniolo, M. Pieruccini, Recrystallization processes in cold-crystallized poly(ethylene terephthalate): interplay between structure evolution and conformational relaxation. Polymer **52**, 3155–3162 (2011)
37. S. Ghosh, A. Sannigrahi, S. Maity, T. Jana, Role of clays structures on the polybenzimidazole nanocomposites: potential membranes for the use in polymer electrolyte membrane fuel cell. J. Phys. Chem. C **115**, 11474–11483 (2011)
38. P.B. Ho, L.H. Chang, S.Y. Joon, L.M. Young, F.D. Benny, K.J. Hyoung, Effect of cross-linked chain length in sulfonated polyimide membranes on water sorption, proton conduction, and methanol permeation properties. J. Membr. Sci. **285**, 432–443 (2006)
39. S. Matiullah, M. Nadeem, M. Atif, Dielectric relaxation with polaronic and variable range hopping mechanisms of grains and grain boundaries in $Pr_{0.8}Ca_{0.2}MnO_3$. J. Appl. Phys. **112**, 103718 (2012)
40. I.M. Javid, M. Nadeem, M.M. Hassan, Low temperature AC electrical study of $Pr_{0.5-x}La_xCa_{0.5}MnO_3(x = 0.0–0.4)$ ceramics by employing impedance spectroscopy. J. Appl. Phys. **114**, 113708 (2013)